Journal of Astronomical Telescopes, Instruments, and Systems

AstronomicalTelescopes.SPIEDigitalLibrary.org

Polarimetric performance of a polarization modulator based on liquid crystal variable retarders for wide acceptance angles

Pilar García Parejo
Alberto Álvarez-Herrero
Gerardo Capobianco
Silvano Fineschi

Pilar García Parejo, Alberto Álvarez-Herrero, Gerardo Capobianco, Silvano Fineschi, "Polarimetric performance of a polarization modulator based on liquid crystal variable retarders for wide acceptance angles," *J. Astron. Telesc. Instrum. Syst.* **5**(3), 034002 (2019), doi: 10.1117/1.JATIS.5.3.034002.

Polarimetric performance of a polarization modulator based on liquid crystal variable retarders for wide acceptance angles

Pilar García Parejo,[a] Alberto Álvarez-Herrero,[b,*] Gerardo Capobianco,[c] and Silvano Fineschi[c]
[a]ISDEFE, INTA, Madrid, Spain
[b]Space Optics Area, Instituto Nacional de Técnica Aeroespacial, INTA, Madrid, Spain
[c]Observatorio Astronomico di Torino, Instituto Nazionale di Astronomia, Pino Torisese, Italy

Abstract. Liquid crystal variable retarders (LCVRs) will be used in the polarization modulation packages (PMPs) of the instruments SO/PHI (Polarimetric and Helioseismic Imager) and METIS/COR (Multielement Telescope for Imaging and Spectroscopy, Coronagraph) of the Solar Orbiter Mission of the European Space Agency (ESA). Optical retarders are dependent on the angle of incidence (AOI). Since the optical retardances during the polarization modulations are optimized for a particular AOI, other angles increase the polarimetric measurement error. Coronagraphs, such as METIS, are characterized by having wide field-of-view (FoV), which involves large incidence angles through the entire instrument. METIS PMP will work with collimated beams and an AOI up to ± 7.0 deg. For this reason, a double LCVR configuration with molecular tilts in opposite directions was selected for METIS PMP, which provides lower angular dependence. The polarimetric performance of the METIS PMP flight model was measured at different AOIs and compared to a single LCVR PMP. The results shown in this paper demonstrate that the functional concept used in METIS guarantees the polarimetric performances at the wide FoV expected in METIS coronagraph. Moreover, a detailed theoretical model is showed and compared to the experimental data, finding successful agreement, which can be very helpful for the design of instruments characterized by wide FoV. [DOI: 10.1117/1.JATIS.5.3.034002]

Keywords: polarimetry; liquid crystal; space mission; solar orbiter; solar corona; solar physics.

Paper 19009 received Jan. 16, 2019; accepted for publication Jul. 30, 2019; published online Aug. 19, 2019.

1 Introduction

Liquid crystal variable retarders (LCVRs) are optical devices that provide a variable optical retardance achieved by the application of electric fields. Traditionally, they have been used as light polarization modulators for polarimetric applications in ground telescopes.[1] For space applications, LCVRs provide many advantages with respect to the traditional rotatory polarizing optics, in particular, low voltage and power requirements, low mass, low volume, large clear apertures, and they avoid the utilization of mechanisms. LCVRs will be used for the first time in a space mission, the Solar Orbiter Mission of the European Space Agency. This mission is a medium-class mission of the Cosmic Vision Program of the European Space Agency (ESA), being developed in collaboration with NASA. The objective of this space mission is to study the Sun and its inner heliosphere at an approach point to the Sun as close as 0.28 AU. In Solar Orbiter, the LCVRs will be used as polarization modulators[2] in 2 of the 10 scientific instruments: SO/PHI (Polarimetric and Helioseismic Imager) and METIS (Multi Element Telescope for Imaging and Spectroscopy, Coronagraph).

SO/PHI[3] is an imaging spectropolarimeter that will acquire high resolution solar magnetograms of the solar surface of the sun. Its polarization modulator package based on LCVRs will carry out complete characterization of the four Stokes parameters of the incoming light $S = (I\,Q\,U\,V)^T$.

On the other hand, METIS[4] consists of a coronagraph instrument for the study and characterization of the linearly polarized solar K-corona in the visible light (VL) band 580 to 640 nm. The polarimetric optical system of METIS comprises polarization optics in "Sernamont configuration," including a bandpass filter (580 to 640 nm); a fixed quarter-wave retarder; a polarization modulation package (PMP) composed of LCVR cells and a linear polarizer. The METIS polarimetric system will measure the Stokes parameters corresponding to the linear components of the polarization of the light (Q, U) coming from the corona of the sun. Coronagraphs are instruments characterized by having a wide field-of-view (FoV). METIS coronagraph is designed to observe the solar corona with an annular FoV from 1.6 to 2.9 deg. METIS PMP[5] will have to work with collimated beams and angles of incidence up to ± 7.0 deg. Polarization optics, in particular retarders, are sensitive to the angle of incidence (AOI) as their optical retardance changes with the incident angle. A variation of the LCVRs optical retardance along the METIS FoV would involve a different modulation matrix for each pixel in the image. This fact in the instrument would involve a calibration pixel-per-pixel, increasing the difficulty of data analysis and resources needed. For this reason, a configuration of double-cell[6] has been selected for the METIS PMP. It consists of two identical antiparallel aligned nematic (APAN) cells stacked together with their LC molecules tilting in opposite directions, which is known to provide a lower angular dependence[7–9] and therefore higher incident acceptance angles.

Polarimetric efficiencies[10] quantify the error propagation level in the determination of each one of the components of the

*Address all correspondence to Alberto Álvarez-Herrero, E-mail: alvareza@inta.es

Stokes vector of the incoming light. A reduction of the polarimetric efficiencies causes the reduction of the signal-to-noise ratio (SNR) of the instrument and therefore of the polarimetric sensitivity. In order to achieve the highest polarimetric sensitivity, the modulation scheme of the PMPs must be carefully selected to give maximum polarimetric efficiencies. In addition, some critical points of the LCVR cells must be taken into consideration during the design of the polarimeter, such as temperature dependence, response times, retardance homogeneity along the clear aperture, chromatism, and retardance dependence on the AOI. These parameters can produce a deviation from the values of the retardances of the optimal modulation scheme, producing a decrease in the polarimetric efficiencies. Due to the wide FoV expected in METIS coronagraph, the retardance dependence on the AOI is one of the most critical points to take into consideration. Along the wide FoV of METIS, a high dependence of the LCVR optical retardance on the AOI would lead to polarimetric images of the solar corona with different sensitivities in the determination of the Stokes parameters of the incoming light.

The aim of this work is to demonstrate quantitatively and from a polarimetric point of view, the advantage of using liquid crystal-based polarization modulators in a double-cell configuration compared to a single-cell configuration for wide acceptance angles. For this, polarimetric performances of the METIS PMP FM and a single-cell PMP have been measured and compared, measuring their modulation matrices (O) and polarimetric efficiencies as a function of the AOI, until 21 deg. In addition, a detailed theoretical model is showed and compared to the experimental data. The other aim of this work is to present a model of the polarimetric performances of liquid crystals polarization modulators as a function of the AOI, which could be very valuable for the design of instruments that are characterized by wide FoV. Based on the model and results shown in this paper, researchers can decide to select polarization modulators based on single or double LCVR cell configuration, depending on their instruments requirements. Moreover, this is the first time that polarization modulators based on liquid crystals will be used in a space instrument, and therefore this work has especial relevance for the design of polarimeters that will be on board future space missions.

2 Theory

2.1 *Polarization Modulation*

Stokes polarimeters are optical instruments that determine the Stokes parameters of the incoming light by its modulation using polarization optics (wave-retarders and polarizers). As detectors are only sensitive to the intensity of light (I), it is necessary to transform the Stokes parameters Q, U, and V into I changes. For this reason, polarization optics is required to affect the polarization state of light, i.e., perform a modulation of the polarization. The polarization detection is as follows:

Incoming light Stokes vector $S = (S_1, S_2, S_3, S_4) = (I\,Q\,U\,V)^T$ is transformed by a polarization modulation M (the Mueller matrix of the polarization modulator) into $S_0 = (I_0\,Q_0\,U_0\,V_0)^T$. However, because only the intensity of I_0 can be measured, we are sensitive to only the first row of M. Therefore, an intensity measurement of the detector is

$$I_0 = \begin{pmatrix} M_{11} & M_{12} & M_{13} & M_{14} \end{pmatrix} \begin{pmatrix} I \\ Q \\ U \\ V \end{pmatrix}, \tag{1}$$

with M_{ij} being the elements of the Mueller matrix M. If the four Stokes parameters of the incoming light are required to be measured, at least four intensity measurements should be carried out. Then, the Mueller matrix of the polarization modulator needs to be changed four times in order to obtain four different intensity measurements. Then, we will have the following system of linear equations:

$$\begin{pmatrix} I_0^{(1)} \\ I_0^{(2)} \\ I_0^{(3)} \\ I_0^{(4)} \end{pmatrix} = \begin{pmatrix} M_{11}^{(1)} & M_{12}^{(1)} & M_{13}^{(1)} & M_{14}^{(1)} \\ M_{11}^{(2)} & M_{12}^{(2)} & M_{13}^{(2)} & M_{14}^{(2)} \\ M_{11}^{(3)} & M_{12}^{(3)} & M_{13}^{(3)} & M_{14}^{(3)} \\ M_{11}^{(4)} & M_{12}^{(4)} & M_{13}^{(4)} & M_{14}^{(4)} \end{pmatrix} \begin{pmatrix} I \\ Q \\ U \\ V \end{pmatrix} = OS, \tag{2}$$

where O is the so-called modulation matrix. Inverting Eq. (2), the incoming light Stokes parameters are obtained as

$$S = O^{-1} \begin{pmatrix} I_0^{(1)} \\ I_0^{(2)} \\ I_0^{(3)} \\ I_0^{(4)} \end{pmatrix} = DI, \tag{3}$$

where D is the demodulation matrix. Then, the polarimetric analysis problem reduces to find the inverse of the matrix O. For a polarization modulator based on LCVRs, the modulation or change of the value of M matrix is achieved by changing the optical retardance value of the LCVRs by the application of different voltages to the LCVRs.

The design of a polarimeter relies on obtaining a modulation scheme whose matrices O give optimally measured Stokes parameters. It is mandatory to have enough different configurations to be able to have an invertible O matrix. This is quantified through the efficiency vector[5] or through the condition number of the demodulation matrix.[11] The efficiency vector gives a measure of the level of error propagation for each one of the components of the Stokes vector. It is known that the efficiency vector for a complete Stokes polarimeter is

$$\varepsilon_i = \left(n \sum_{j=1}^{n} D_{ij}^2 \right)^{-1/2}, \tag{4}$$

where n is the measurement number and i goes from 1 to 4 (corresponding to the four Stokes parameters). Theoretical considerations[5] show that the maximum obtainable polarimetric efficiencies of a modulation scheme is given by $\varepsilon_{\max,1} = 1$ and $\sum_{i=2}^{4} \varepsilon_{\max,i}^2 = 1$.

The SNR of the instrument is related to the polarimetric efficiencies as follows. The SNR of the Stokes parameter S_1 is related to the single-shot s/n through $(S/N)_1 = (s/n)\varepsilon_1 (N_p N_a)^{-1/2}$, where N_p and N_a are the number of single detector shots and the accumulations number, respectively, as explained in Ref. 12. Then, the SNR for Stokes $S_{2,3,4}$ can be

calculated using the relationship $(S/N)_I = \varepsilon_i/\varepsilon_1(S/N)_1$. Maximizing the polarimetric efficiency for each Stokes parameter involves maximizing the SNR to determine each specific Stokes parameter, and this is the reason why the modulation scheme must be selected to achieve maximum polarimetric efficiencies.

A complete Stokes polarimeter measures the four Stokes parameters of the incoming light. A very common configuration for these instruments consists in using a dual configuration of LCVR cells with their optical axes properly oriented at 0 deg and 45 deg. If this type of polarimeter requires obtaining uniform efficiencies in the Stokes parameters: Q, U, and V, the maximum achievable polarimetric efficiency of the modulation scheme is

$$\begin{aligned}\varepsilon_{\max} &= (\varepsilon_1 \quad \varepsilon_2 \quad \varepsilon_3 \quad \varepsilon_4) = (1 \quad 1/\sqrt{3} \quad 1/\sqrt{3} \quad 0) \\ &\approx (1 \quad 0.577 \quad 0.577 \quad 0.577). \end{aligned} \tag{5}$$

The polarimeter of METIS is a partial Stokes polarimeter, which means that it determines the linear polarization components of the Stokes parameters of the incoming light (Q and U). Then, the objective is to obtain maximum polarimetric efficiencies for linear polarization (Q and U) being the modulation efficiency of the circular polarization (V) not relevant. Therefore, the modulation scheme must be selected complying with the following maximum achievable polarimetric efficiencies:

$$\begin{aligned}\varepsilon_{\max} &= (\varepsilon_1 \quad \varepsilon_2 \quad \varepsilon_3 \quad \varepsilon_4) = (1 \quad 1/\sqrt{2} \quad 1/\sqrt{2} \quad 0) \\ &\approx (1 \quad 0.707 \quad 0.707 \quad 0). \end{aligned} \tag{6}$$

These polarimetric efficiencies are achieved by using a quarter-waveplate with its fast axis at 0 deg and one LCVR with its fast axis at 45 deg followed by a linear polarizer at 0 deg, which is the optical configuration for METIS. If not fixed quarter-wave is used, then the lineal equation system obtained would allow determining the circular polarization component (V) instead of linear component U, achieving maximum efficiency 0.707 for ε_4, instead of ε_3.

As the number of Stokes parameters required is three, the minimum intensity measurements required for METIS are three. Nevertheless, a larger number of modulations can be performed to minimize the error in the measurements. For METIS, a modulation scheme of four intensity measurements has been selected being the modulation matrix as follows:

$$O = \begin{pmatrix} 1 & \cos\Delta\varphi_1 & \sin\Delta\varphi_1 \\ 1 & \cos\Delta\varphi_2 & \sin\Delta\varphi_2 \\ 1 & \cos\Delta\varphi_3 & \sin\Delta\varphi_3 \\ 1 & \cos\Delta\varphi_4 & \sin\Delta\varphi_4 \end{pmatrix}, \tag{7}$$

where $\Delta\varphi_i$ are the retardances of the LCVR cells. The fourth column of the modulation matrix is zero, as the polarimetric system proposed is not sensitive to V polarization states.

One of the LCVR optimum retardances set that gives the maximum polarimetric efficiencies is one that differs by 90 deg, which was the modulation scheme proposed for METIS. As two LCVR cells in parallel are used in METIS (with their tilts in opposite direction), the optical retardances are the sum of the retardances of the individual cells. Therefore, the LCVRs retardances selected for achieving the maximum polarimetric efficiencies are given in Table 1.

Table 1 Modulation scheme for the METIS PMP (double-cell configuration).

Retardances (deg)	PM_1	PM_2	PM_3	PM_4
LCVR1	180	135	90	45
LCVR2	180	135	90	45
Total	360	270	180	90

PM, polarization modulation

For the case of a single-cell PMP, the optical retardances required for the LCVR cell are given in Table 2

In both modulation schemes, the retardances changes are carried out from higher to lower values, which involves going from lower to higher voltages. In this way, the LCVR response times are minimized during the polarization modulation.

Therefore, considering the Müller matrix of the ideal polarizing elements of the system and normalizing to the first element, the modulation and demodulation matrixes are

$$O = \begin{pmatrix} 1 & 1 & 0 \\ 1 & 0 & -1 \\ 1 & -1 & 0 \\ 1 & 0 & 1 \end{pmatrix} \quad D = \begin{pmatrix} 0.25 & 0.25 & 0.25 & 0.25 \\ 0.5 & 0 & -0.5 & 0 \\ 0 & -0.5 & 0 & 0.5 \end{pmatrix}.$$

The optical retardances shown in Tables 1 and 2 give the maximum achievable polarimetric efficiencies. Nevertheless, in real systems, deviations from these optimum optical retardances occur and must be taken into account in the design of the polarimeter. LCVRs will present different manufacturing imperfections, such as optical activity or depolarization. The manufacturing tolerances of the mechanical elements will produce azimuth or tilt angles between the polarizing elements (LCVRs, polarizers, etc.) different with respect to the designed values.[13] Critical points such as the dependence of retardance on temperature, retardance homogeneity along clear aperture, response times, chromatism, and dependence of the retardance on the AOI must be taken into account. Among others, the more specific critical points that need to be analyzed for the METIS instrument are chromatism and dependence on the AOI.

The spectral range for the METIS instrument is from 580 to 640 nm. The LCVRs wavelength dependence was studied and the resulting contrast of the corona measurements fulfils the scientific requirements. Nevertheless, this is beyond the scope of this paper. In this work, a light of wavelength around the center of the METIS spectral range (617 nm) and with a bandwidth of 10 nm has been used for the measurement of the polarimetric efficiencies.

Table 2 Modulation scheme for a PMP with single-cell configuration.

Retardances (deg)	PM_1	PM_2	PM_3	PM_4
LCVR	360	270	180	90

PM, polarization modulation

In this paper, the dependence on the AOI has been thoroughly studied experimentally and theoretically. The theoretical model used is presented in Secs. 2.2 and 2.3.

2.2 *LCVRs Dependence on Incident Angle*

The LCVRs have a well-known AOI dependence since they are anisotropic materials that can be considered as uniaxial material whose optical axis changes with the application of voltage. The AOI dependence for anisotropic materials was well established by Veiras et al.[14] They are provided with a general formula that relates the optical retardance introduced by a uniaxial plane-parallel plate with arbitrary orientation of its optical axis when the incident wave has an arbitrary direction

$$\Delta\varphi = \frac{2\pi L}{\lambda}\left((n_o^2 - n^2\sin^2\alpha)^{1/2} + \frac{n(n_o^2 - n_e^2)\sin\theta\cos\theta\cos\delta\sin\alpha}{n_e^2\sin^2\theta + n_o^2\cos^2\theta} + \frac{-n_o\{n_e^2(n_e^2\sin^2\theta + n_o^2\cos^2\theta - [n_e^2 - (n_e^2 - n_o^2)\cos^2\theta\sin^2\delta]n^2\sin^2\alpha\}^{1/2}}{n_e^2\sin^2\theta + n_o^2\cos^2\theta}\right), \tag{8}$$

where $\Delta\varphi$ is the waveplate optical retardance, L is the thickness of the LC layer, λ is the light wavelength, n_o and n_e are the ordinary and extraordinary refractive indices of the LC molecules, respectively, n is the refractive index of the material before reaching the LC layer, α is the AOI, and θ is the angle between the optical axis and the interface. α and θ are shown in Fig. 1(a). δ is the angle between the plane of incidence and the optical projection on the interface (azimuth). δ is 0 deg and 90 deg when the AOI is varied along the extraordinary and ordinary refractive index of the liquid crystal molecules, respectively. The extraordinary refractive index direction of the liquid crystal molecules corresponds to their molecular long axis direction as shown in Fig. 1(b).

Angle θ for an LCVR device corresponds to the tilt of molecules, which is changed by the application of voltage. For simplifying our calculations, we assume that the applied voltage to the LCVR induces a homogeneous tilt of the molecules across the cell. This approximation involves a mean tilt (θ) of the LC molecules. This means tilt can be calculated as

$$\Delta\varphi = \frac{2\pi L}{\lambda}(\overline{n}_e - n_o), \tag{9}$$

$$\overline{n}_e = \frac{n_o n_e}{(n_e^2\sin^2\theta + n_o^2\cos^2\theta)^{1/2}}, \tag{10}$$

where $\overline{n}_e$ is the effective extraordinary refractive index. Solving Eq. (10), the mean tilt (θ) can be calculated from

$$\theta = \arcsin\left[\sqrt{\frac{n_o^2 n_e^2}{\overline{n}_e^2(n_e^2 - n_o^2)} - \frac{n_o^2}{(n_e^2 - n_o^2)}}\right]. \tag{11}$$

Therefore, the mean tilt of the LC molecules can be calculated knowing the terms n_o, n_e, and $\overline{n}_e$.

2.3 *Theoretical Simulations*

Theoretical simulations have been performed using as input, known data of the LCVR cells characterized in this paper at normal incidence (see Sec. 3.1), which are standard measurements. Then, the dependence of the optical retardance on the AOI is calculated theoretically from Eq. (8). The parameters needed in this equation are obtained as follows:

The mean tilt (θ) of the molecules is obtained from Eq. (11) at the LCVRs optical retardances required for the modulation scheme of the PMPs (Tables 1 and 2). For this, $\overline{n}_e$ is needed and is obtained from the optical retardance versus Voltage curves measured for the LCVRs at normal incidence during the calibration process (see Fig. 6 in Sec. 3.2) using Eq. (9). The wavelength measured was 617.3 nm. N_e and n_o of LC the mixture ZLI-3700-000 (outside of the LCVR cell) at 617.3 nm were obtained from measuring in an Abbe refractometer[15] with an accuracy of 0.0001. The LC molecules were aligned perpendicular to the main and secondary prism surfaces of an Abbe refractometer by coating these two surfaces with a solution of 0.294 wt. % of surfactant hexadecyltrimethyl-ammonium bromide dissolved in methanol. Both n_e and n_o are obtained through a polarizing eyepiece of the refractometer. Thickness of the LCVR cells has been estimated. LCVRs manufacturer use spacers to create the cavity where the LC molecules are located. In this case, the manufacturer use spacers that have a diameter around 10 μm; therefore, a cavity thickness close to 10 μm is expected. Nevertheless, the manufacturing process can produce deviation from this ideal thickness. If this theoretical value of thickness is considered in the calculations, this produces excessive errors in the tilts estimation. The pretilt obtained (tilt of the molecules at zero volts) can have no physical meaning or to be higher than expected. By manufacturing processes, these devices present pretilts between 1 deg and 3 deg. Simulations using thicknesses that give pretilts between 1 deg and 5 deg were done, and no significant changes were observed in the results. Therefore, the simulations for the polarimetric performance

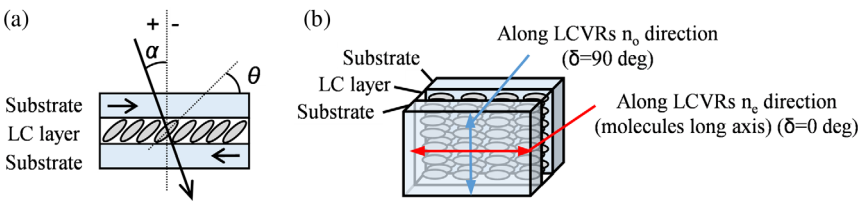

Fig. 1 Angles scheme: (a) side view of the LCVR. (b) View from above of the LCVR.

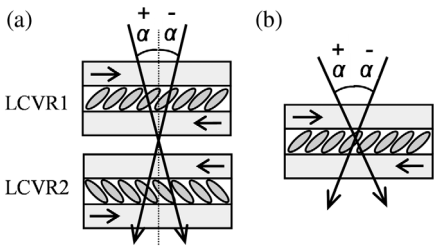

Fig. 2 (a) PMP with double-cell configuration (METIS PMP) with the molecular tilts in opposite directions. (b) PMP with single-cell configuration.

presented in this work have been done considering LCVR thicknesses (between 9 and 9.15 μm) that give pretilts of 1 deg.

The theoretical simulations have been performed along the extraordinary ($\delta = 0$) and ordinary ($\delta = 90$) refractive index at angles of incidence (α) between -21 deg and $+21$ deg and, for a configuration of single and double cell PMP. Note that, simulations for a PMP with double cell are performed using molecular tilts (θ) in opposite directions as METIS configuration and as schemed in Fig. 2.

Once we theoretically calculated the optical retardance of the LCVR cells as a function of the AOI, we can calculate the elements of the matrix O as well as the dependence of the polarimetric efficiencies as a function of the AOI from Eqs. (6) and (4), respectively.

We have simulated a polarimetric system, which includes the PMP (single- or double-cell configuration) and a polarizer analyzer. Not quarter-wave plate is included, which means that we will obtain maximum efficiency for the circular polarization component (V) instead of linear component U and maximum efficiency 0.707 for ε_4 instead ε_3. Nevertheless, mathematically, if the quarter-wave plate is not used, we will obtain the same modulation matrix O as Eq. (6) but with the third column as zeros and fourth column depending on retardance as sin $\Delta\varphi_i$. Discarding the column of zeros, the modulation matrix will be the same for both cases and the values of ε_4 will be equivalent to ε_3.

We have simulated this system, as the measurements presented in this paper were done without quarter-wave plate. Experimentally, a quarter-wave plate can introduce nonidealities in the polarimetric system that could be attributed to the PMPs. For this reason, the use of a quarter-wave plate was discarded. Then, the polarimetric efficiencies calculated in this section corresponds to [ε_1, ε_2, ε_4]. In addition, we have calculated the total polarimetric efficiency defined as $\varepsilon_{\text{Total}} = \sqrt{\varepsilon_2^2 + \varepsilon_4^2}$, whose maximum theoretical value is 1.

The results of the simulations are shown in Fig. 3 (modulation matrix) and Fig. 4 (polarimetric efficiencies). Different conclusions can be extracted from them:

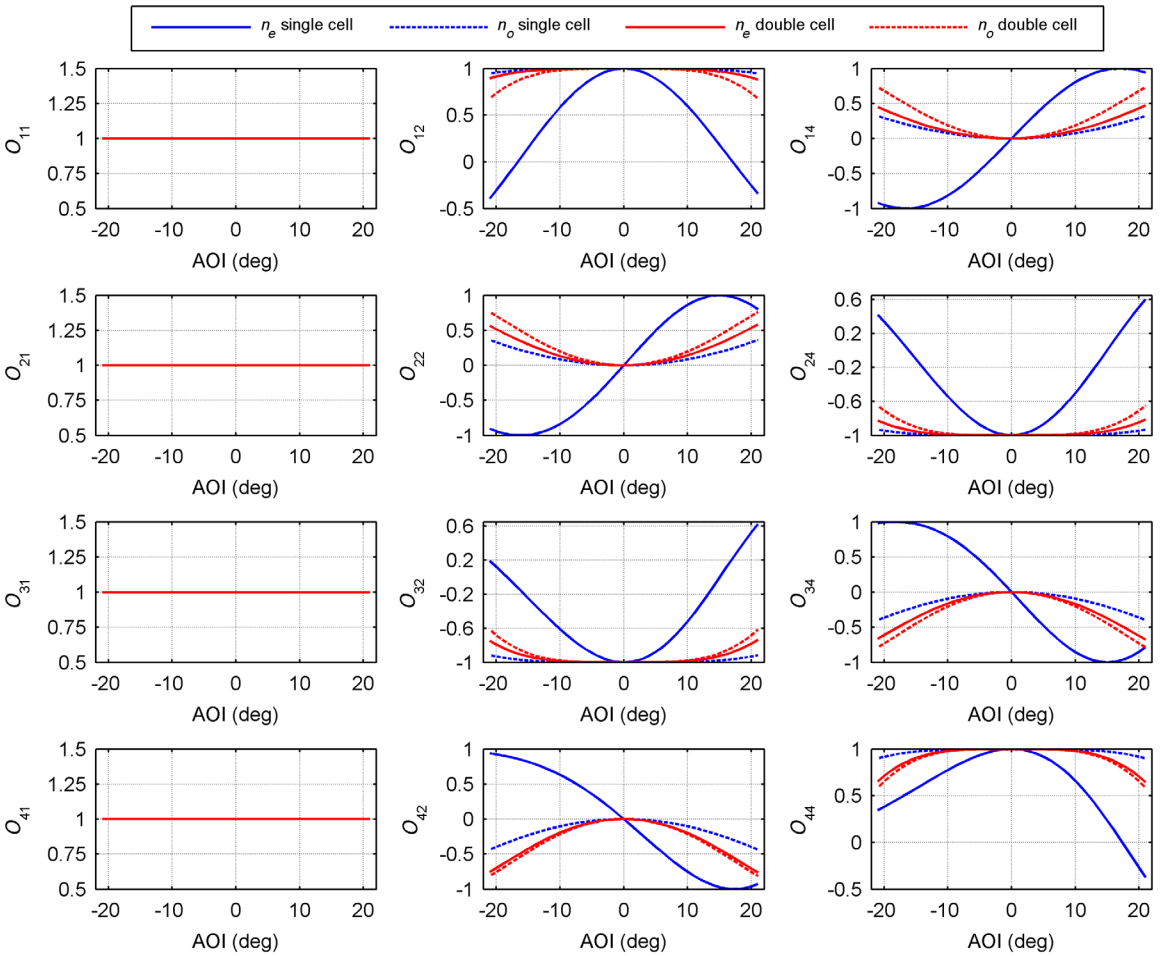

Fig. 3 Comparison between modulation matrix O elements of the PMPs with single- and double-cell configurations along extraordinary and ordinary refractive index directions.

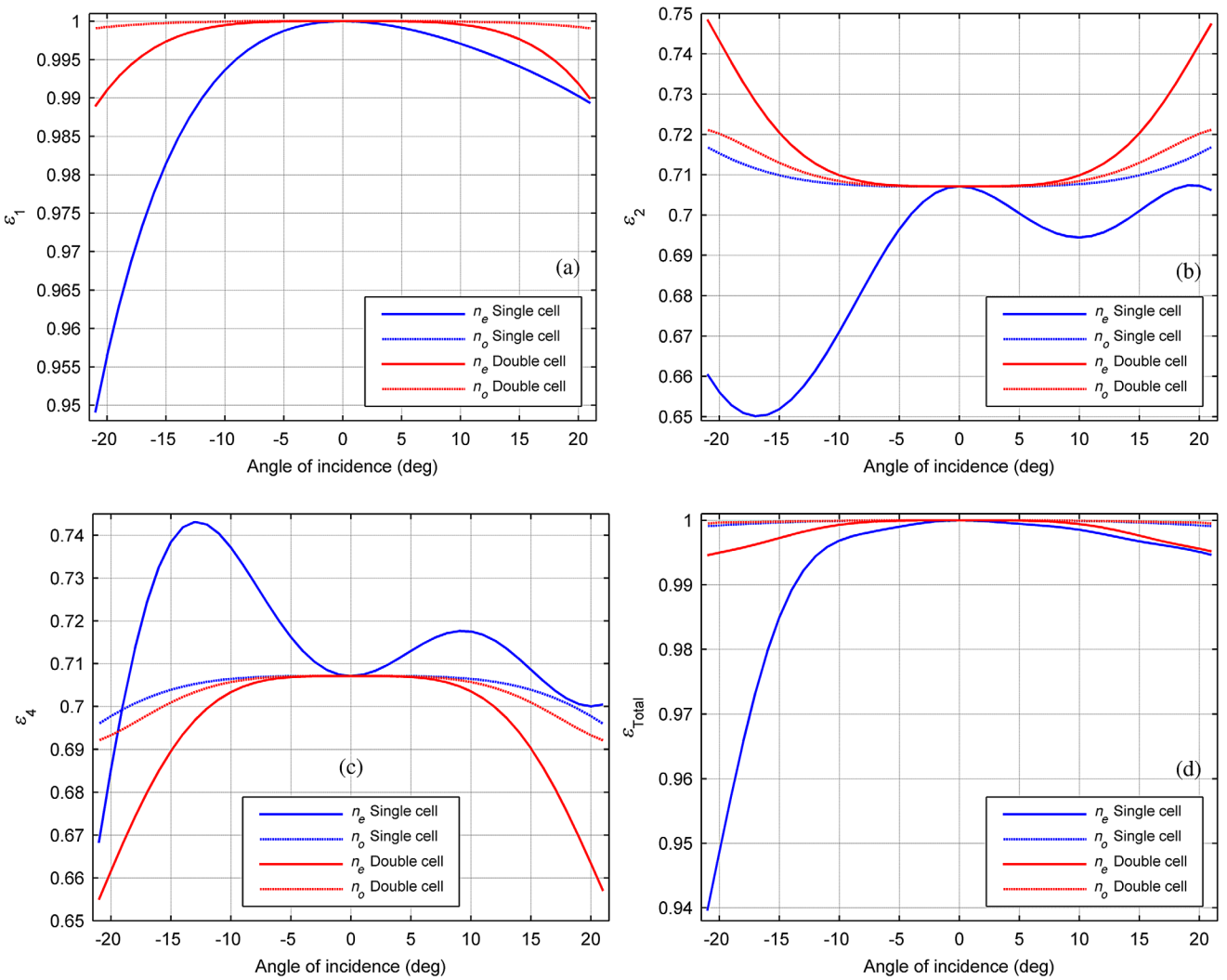

Fig. 4 Comparison between polarimetric efficiencies PMPs with single- and double-cell configurations along extraordinary and ordinary refractive index direction. (a) ε_1, (b) ε_2, (c) ε_4, and (d) ε_{total}.

- The use of a double-cell PMP with their molecular tilts in the opposite direction drastically reduces the dependence on the AOI along the extraordinary refractive index when compared to a single-cell PMP, which in fact is the functional concept of the METIS PMP. Opposite behavior is found along the ordinary refractive index. Nevertheless, this effect is much lower. This is explained by the fact that the optical compensation produced by using double cells with their tilts in opposite directions is achieved exclusively along the extraordinary refractive index direction not the ordinary refractive index. Along the ordinary refractive index direction, having two LCVR cells involves to have twice the thickness. The higher the thickness the higher the dependence on angle.
- For both single- and double-cell PMPs, the polarimetric efficiencies dependence on the AOI (Fig. 4) are much higher along the extraordinary refractive index than along the ordinary refractive index direction. Nevertheless, for the case of the elements of the modulation matrix (Fig. 3) in the double-cell configuration, the dependence is higher along the ordinary refractive index direction.
- An asymmetric behavior between negative and positive angles of the AOI is found for the case of the single-cell PMP along the extraordinary refractive index direction. This is due to the intrinsic asymmetric geometry of the system for incident rays [see Fig. 2(b)] that comes from the elongated shape of the molecule responsible for its birefringence. Along the ordinary refractive direction, this asymmetry does not exist. For the case of the PMP with double-cell configuration, the symmetry is obtained when the LCVR cells are modulated at the same molecular tilts. If the LCVR cells are very similar and they are modulated at the same optical retardances (as METIS PMP case), the symmetry is observed and the reduction of the dependence on the AOI is achieved.

Considering the previous, the polarimetric measurements of the PMPs studied in this work were done along the extraordinary refractive index direction. On one hand, a much higher dependence on the AOI for both PMPs along this direction is found. On the other hand, the functional concept of METIS PMP will be demonstrated comparing the polarimetric performances of the METIS PMP FM with respect to a single-cell PMP. In addition,

the measurements were done from zero to negative angles of incidence, which is the worst case, i.e., higher dependence on the AOI is expected for the case of single-cell configuration.

3 Experimental

3.1 *METIS Polarization Modulation Package Description*

3.1.1 *LCVR cells design*

The architecture for the LCVR cells is APAN using the positive nematic liquid crystal mixture ZLI-3700-000. The LCVR cell design consists of two fused silica glass substrates of 5 mm coated for one side with a transparent conducting material (ITO) and the other side with an antireflective coating optimized in the working range of METIS (580 to 640 nm). On top of the ITO layer, an alignment layer consisted of rubbed polyimide (PI-2545) is deposited, which provides the initial alignment of the LC molecules inside the cell. The glass substrates are hold apart by a mixture of glass fiber spacers, which diameter defines the thickness of the LC layer and adhesive, which will be the adhesion point between the two substrates (gasket). In this case, glass fiber spacers of 10 μm were used. The cell is assembled and partially sealed to let an opening for LC filling. The LC is filled by vacuum filling and finally the cell is completely sealed with glue (stopper). An external part of the ITO electrode is electrically connected to the driver.

3.1.2 *METIS PMP design (double-cell configuration)*

The PMP of METIS consists of two identical APAN cells placed parallel but with their LC molecules tilts in opposite directions. The voltage is applied to the LC cells through a kapton flexible cable adhered to the cells. In addition, the cable includes a signal for the temperature sensor (PT100), which allows knowing the temperature of the cell for the active thermal control. The LCVR cells are mounted in aluminum rings and a heater for each cell is attached to them to provide the heating power. The active thermal control is driven using a proportional-integral-derivative algorithm in order to obtain a suitable repeatability of the LCVRs optical retardance. The main structure for the PMP of METIS is made of titanium. An exploited scheme of the design of the PMP model and the flight model of the METIS PMP is shown in Fig. 5 and explained in Ref. 2.

3.1.3 *PMP with single-cell configuration*

The PMP with single-cell configuration presented in this paper consists of an LCVR cell with the same design as specified in section LCVR cell design, i.e., the same as used in METIS PMP FM. In this case, the thermal control is achieved by using laboratory thermal components (temperature sensors and heaters). The same electronic and thermal equipment as METIS PMP FM is used to control voltage and temperature.

3.2 *Calibration*

The purpose of the calibration of a polarimetric instrument as METIS is to obtain the modulation matrix O of the complete polarimeter, which includes the fixed quarter-wave plate, the METIS PMP, and the analyzer (linear polarizer). The resulting modulation matrix O and its inverse matrix D will define the polarimetric efficiencies [according to Eq. (4)], and therefore the polarimetric sensitivity of the polarimeter to measure the Stokes parameters of the incoming light. Nevertheless, before its integration in the complete polarimeter, the METIS PMP needs to be calibrated characterizing their modulation matrices and polarimetric efficiencies in order to verify its proper performance. The calibration is performed using laboratory polarization components (quarter wave-plates and polarizers) with previous characterized optical properties. The calibration of the PMP follows a two-step process. The first step consists of the individual characterization of the two LCVRs composing the PMP (or one LCVR cell for the case of the PMP with a single-cell configuration). The second step includes the determination of the modulation matrix of the system using a polarization state generator (PSG), which introduces known polarization states. The process is described in the following sections:

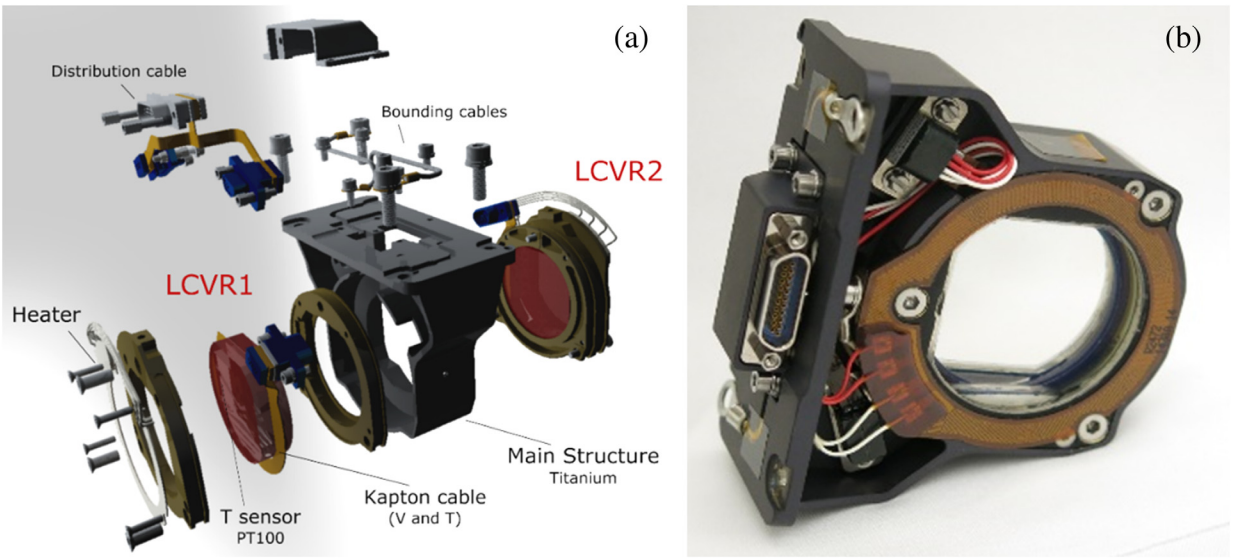

Fig. 5 (a) Exploited scheme of the design of the METIS PMP. (b) Front view of PMP FM of the METIS instrument.

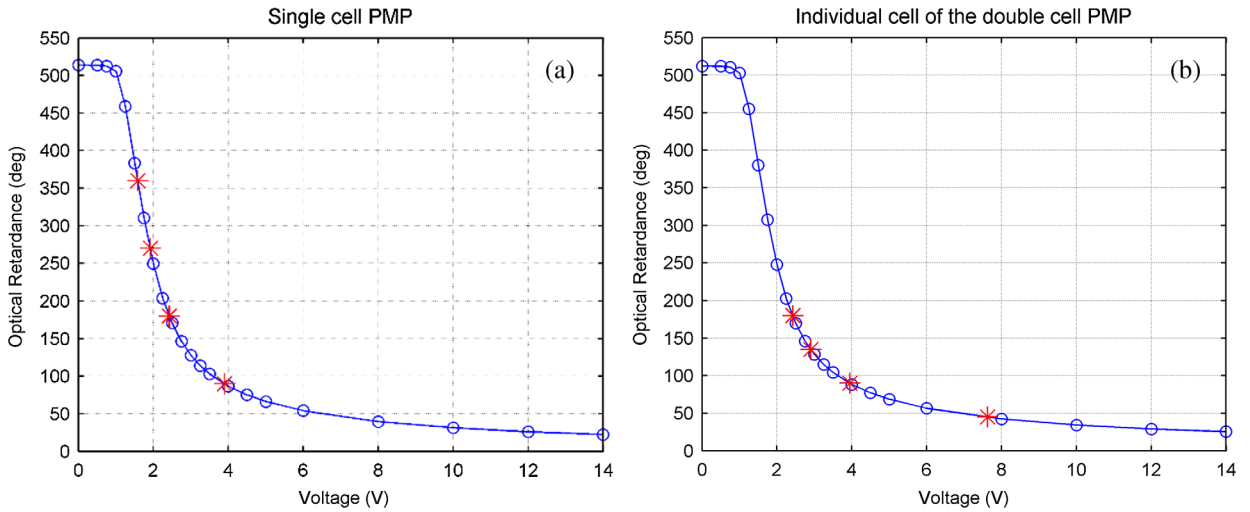

Fig. 6 Optical retardance versus voltage for single- and double-cell configuration PMPs at 40°C. Red markers correspond to the retardances of the modulation scheme. (a) 360 deg, 270 deg, 180 deg, and 90 deg for single-cell configuration. (b) 180 deg, 135 deg, 90 deg, and 45 deg for one of the cells of the PMP with double-cell configuration.

3.2.1 *Calibration of the LCVR cells*

The calibration of the LCVRs consisted of the measurement of the optical retardance of each LCVR cell at different voltages at controlled temperature, as shown in Fig. 6. These measurements were carried out in a Woollam variable angle spectroscopic ellipsometer with an accuracy in the optical retardance of 0.1 deg. The calibration of the PMP and single LCVR cell shown in this paper is at 40°C. Nevertheless, for METIS PMP FM, the optical retardance as a function of voltage was measured at eight temperatures in a temperature range between 30°C and 80°C. The voltage values for each cell corresponding to the optical retardances of the optimized modulation scheme (Table 1) are obtained by interpolation of these curves as shown in Fig. 6. Then, each LCVR cell will be modulated at these voltages. After the calibration, the two LCVR cells are placed in the mechanical structure where they are aligned parallel to each other but with their LC molecules tilts in opposite directions in order to achieve the required reduction of the dependence on the AOI.

3.2.2 *Optical set-up for the calibration of the METIS PMP*

The calibration of the METIS PMP was performed using the set-up shown in Fig. 7, where P1 is a linear polarizer, QWP is the quarter-wave plate at the wavelength used (617 nm), L1 is a lense with a focal length of 200 that produces collimated beams, PMP is the PMP (single- or double-LCVR cell configuration),

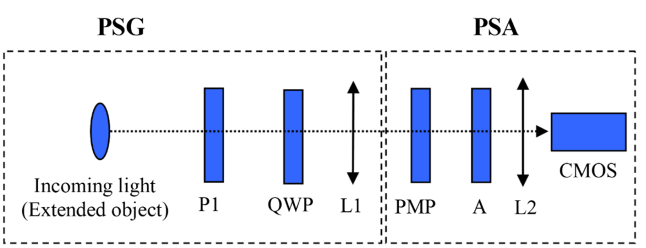

Fig. 7 Optical set-up for the calibration of the PMPs.

A (analyzer) is a linear polarizer, and L2 is a lense that generates the image of the extended object in the camera (CMOS). PSG corresponds to polarization state generator, and PSA to polarization state analyzer. The PMP is rotated 45 deg with respect to the analyzer.

For the calibration it is necessary to introduce 73 known polarization states of the light, which is performed using the PSG, consisting in a polarizer followed by a QWP at different azimuthal angles. Defining a known input S_j Stokes vector as $S_j = (1\, Q_j\, U_j\, V_j)^T$ generated by the PSG, and the corresponding measured intensity as I_j, the calibration for the i'th modulation matrix row is described as

$$\begin{pmatrix} I_1^i \\ I_2^i \\ I_3^i \\ I_4^i \end{pmatrix} = \begin{pmatrix} 1 & Q_1 & U_1 & V_1 \\ 1 & Q_2 & U_2 & V_2 \\ \vdots & \vdots & \vdots & \vdots \\ 1 & Q_n & U_n & V_n \end{pmatrix} \begin{pmatrix} O_{i1} \\ O_{i2} \\ O_{i3} \\ O_{i4} \end{pmatrix} \equiv I^i = SO_i. \tag{12}$$

A simple inversion of matrix S gives the modulation matrix elements corresponding to the state i:

$$O_i = S^{-1} I^i. \tag{13}$$

The determination of the modulation matrix is performed pixel-per-pixel, i.e., each pixel in the image has a calculated modulation matrix. An inversion of the modulation matrix O gives the demodulation matrix D. Then, the polarimetric efficiencies are calculated using Eq. (4). Since no quarter-wave plate is included in the PSA, we have no sensitivity to U polarization states but to V polarization states, and therefore the polarimetric efficiencies calculated will be $[\varepsilon_1, \varepsilon_2, \varepsilon_4, \varepsilon_{\text{Total}}]$, where the maximum theoretical values are [1, 0.707, 0.707, 1].

The optical setup is in collimated configuration as in the METIS instrument. A calibrated grid in the extended diffused object was used in order to determine the different angles of incidence in the image. An optimized image quality area was selected, as shown in Fig. 8. The area selected corresponds

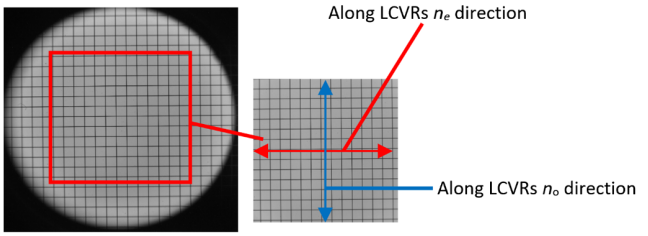

Fig. 8 Calibrated grid in the extended object (±2-deg FoV).

to angles of ±2 deg (the period grating is 1 mm, and 7 mm corresponds to 2 deg of the AOI). The modulation matrix and polarimetric efficiencies were calculated in this area of the image. The directions corresponding in the image to the LCVRs extraordinary and ordinary refractive indices are specified in Fig. 8. These experimental data are shown in Sec. 4.1.

Due to limitations in the optical set-up, no higher angles than ±2 deg of FoV could be achieved. For this reason, the PMP was rotated up to −21 deg along the extraordinary refractive index in order to analyze the behavior of the PMPs at higher values of the AOI. Then, the modulation matrix and polarimetric efficiencies are calculated for these different angles. In this case, the experimental data shown belong to the central pixel of the image, which corresponds to FoV of 0 deg and AOI between 0 and −21 deg along the extraordinary refractive index direction of the LCVRs. These data are shown in Sec. 4.2.

The comparison between the experimental data and the simulations explained in Sec. 2.2 is shown in Sec. 4.3.

4 Results and Discussion

4.1 *Polarimetric Performances of the PMPs Along ± 2 deg FoV and AOI = 0*

The polarimetric measurements shown in this section corresponds to the optimized quality area shown in Fig. 8 with FoV angles up to ±2 deg. Each pixel has a calculated O matrix. Then, the polarimetric efficiencies are also calculated for each image pixel using Eq. (4).

As representative value, the mean modulation matrices for both PMPs are presented

$$O_{\text{single\_cell}} = \begin{pmatrix} 1.024 & 0.873 & -0.279 \\ 0.982 & 0.074 & -0.952 \\ 1.006 & -0.975 & -0.003 \\ 0.988 & 0.039 & 0.972 \end{pmatrix}, \quad \text{std}_{\text{single\_cell}} = \begin{pmatrix} 0.001 & 0.025 & 0.088 \\ 0.002 & 0.097 & 0.016 \\ 0.003 & 0.021 & 0.085 \\ 0.001 & 0.044 & 0.009 \end{pmatrix},$$

$$O_{\text{double\_cell}} = \begin{pmatrix} 1.022 & 0.889 & -0.218 \\ 0.983 & -0.157 & -0.949 \\ 1.004 & -0.953 & 0.151 \\ 0.991 & 0.174 & 0.957 \end{pmatrix}, \quad \text{std}_{\text{double\_cell}} = \begin{pmatrix} 0.001 & 0.019 & 0.008 \\ 0.002 & 0.012 & 0.006 \\ 0.001 & 0.004 & 0.006 \\ 0.002 & 0.005 & 0.002 \end{pmatrix}.$$

These mean O matrices are calculated from the average of all modulation matrices of all the pixels in the image. The standard deviation (std) with respect to these mean values is also shown. It can be observed that the standard deviation values are much higher for the single cell PMP, involving a variation of the LCVRs retardance along FoV higher than for double cell PMP, as expected.

On the other hand, the efficiencies ε_1, ε_2, ε_4, and $\varepsilon_{\text{Total}}$ for single- and double-cell PMPs for each pixel are shown in Fig. 9. The mean values specified in the figures correspond to the average of all the pixels along the clear aperture. The same scale with respect to these mean values has been used in order to compare the performance of the two PMPs along the angles of the FoV.

Several issues can be extracted from the images. First, the dependence on the angle along the extraordinary refractive index is much higher for PMP with single-cell configuration. On the other hand, a slighter dependence on the angle is observed along the ordinary refractive index for the case of the PMP with double-cell configuration. The second thing is that we observe that in general, the standard deviations with respect to the mean value are higher for the case of the PMP with single-cell configuration, which implies a large dependence on the AOI for single-cell PMP. Very significant is the case of ε_4.

4.2 *Polarimetric Performances of the PMPs versus AOI (FoV = 0 Corresponding to Image Central Pixel)*

In this section, we present the polarimetric performances of both PMPs for the central pixel of the image (FoV = 0) and different AOIs along the extraordinary refractive index. The modulation matrices are shown in Table 3. To evaluate the goodness of the modulation matrix obtained experimentally at different AOIs (O_{AOI}), we have computed the root mean square error (RMSE) as figure of merit,[10] defined as

$$\text{RMSE} = \sqrt{\frac{\Sigma_{ij}[(O_{\text{ideal}})_{ij} - (O_{\text{AOI}})_{ij}]^2}{3 \times 4}}. \tag{13}$$

This figure of merit quantifies the difference between O matrices obtained experimentally at a different AOI with respect to the ideal modulation matrix. The values of RMSE for both PMPs as a function of the AOI are shown in Fig. 10.

Both PMPs show similar and low RMSE at zero degrees of the AOI. An RMSE of zero degrees would involve that we have obtained the ideal modulation matrix. Nevertheless, in real systems, deviations from the theoretical values occur. As said before, manufacturing tolerances of the optical and mechanical elements and tolerances of the azimuths angles between

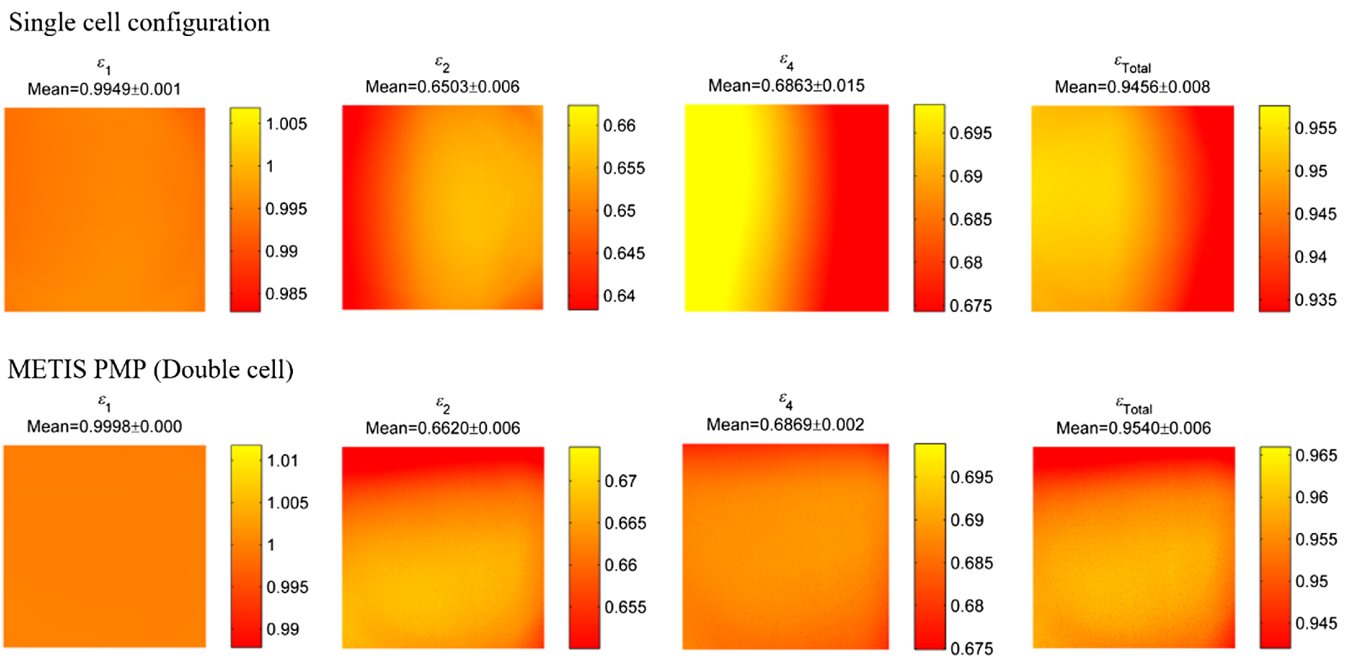

Fig. 9 Modulation efficiencies for single-cell PMP and METIS PMP (double-cell) along ±2-deg FoV.

Table 3 Modulation matrices O measured experimentally at different AOI for PMP with single- and double-cell configurations.

AOI	Single cell	Double cell
0 deg	$O=\begin{pmatrix}1.024 & 0.877 & -0.283\\ 0.982 & 0.069 & -0.962\\ 1.006 & -0.991 & -0.002\\ 0.988 & 0.035 & 0.979\end{pmatrix}$ RMSE = 0.0933	$O=\begin{pmatrix}1.021 & 0.901 & -0.221\\ 0.983 & -0.152 & -0.954\\ 1.005 & -0.954 & 0.150\\ 0.991 & 0.173 & 0.958\end{pmatrix}$ RMSE = 0.1085
−3.5 deg	$O=\begin{pmatrix}1.014 & 0.774 & -0.535\\ 0.984 & -0.209 & -0.931\\ 1.008 & -0.940 & 0.244\\ 0.993 & 0.180 & 0.959\end{pmatrix}$ RMSE = 0.2008	$O=\begin{pmatrix}1.022 & 0.901 & -0.206\\ 0.983 & -0.137 & -0.957\\ 1.005 & -0.956 & 0.131\\ 0.990 & 0.153 & 0.961\end{pmatrix}$ RMSE = 0.0991
−7 deg	$O=\begin{pmatrix}1.005 & 0.602 & -0.744\\ 0.991 & -0.477 & -0.827\\ 1.006 & -0.845 & 0.463\\ 0.998 & 0.297 & 0.932\end{pmatrix}$ RMSE = 0.3285	$O=\begin{pmatrix}1.022 & 0.902 & -0.172\\ 0.983 & -0.092 & -0.958\\ 1.005 & -0.956 & 0.081\\ 0.990 & 0.096 & 0.967\end{pmatrix}$ RMSE = 0.0759
−10.5 deg	$O=\begin{pmatrix}0.997 & 0.378 & -0.887\\ 0.999 & -0.697 & -0.660\\ 1.002 & -0.717 & 0.643\\ 1.002 & 0.384 & 0.902\end{pmatrix}$ RMSE = 0.4495	$O=\begin{pmatrix}1.022 & 0.905 & -0.104\\ 0.984 & -0.011 & -0.957\\ 1.004 & -0.951 & -0.019\\ 0.989 & -0.018 & 0.963\end{pmatrix}$ RMSE = 0.0474
−14 deg	$O=\begin{pmatrix}0.990 & 0.115 & -0.972\\ 0.997 & -0.843 & -0.428\\ 0.999 & -0.560 & 0.801\\ 1.014 & 0.417 & 0.876\end{pmatrix}$ RMSE = 0.5620	$O=\begin{pmatrix}1.0224 & 0.915 & -0.024\\ 0.986 & 0.094 & -0.957\\ 1.003 & -0.937 & -0.149\\ 0.989 & -0.168 & 0.942\end{pmatrix}$ RMSE = 0.0800
−17.5 deg	$O=\begin{pmatrix}0.980 & -0.167 & -0.941\\ 1.005 & -0.970 & -0.192\\ 1.002 & -0.395 & 0.879\\ 1.012 & 0.505 & 0.842\end{pmatrix}$ RMSE = 0.6621	$O=\begin{pmatrix}1.021 & 0.916 & 0.093\\ 0.988 & 0.238 & -0.938\\ 1.000 & -0.891 & -0.326\\ 0.990 & -0.372 & 0.876\end{pmatrix}$ RMSE = 0.1706
−21 deg	$O=\begin{pmatrix}0.991 & -0.434 & -0.873\\ 1.008 & -0.991 & 0.058\\ 0.994 & -0.232 & 0.955\\ 1.007 & 0.530 & 0.834\end{pmatrix}$ RMSE = 0.7488	$O=\begin{pmatrix}0.995 & 0.931 & 0.216\\ 1.008 & 0.369 & -0.873\\ 1.026 & -0.824 & -0.495\\ 0.970 & -0.561 & 0.722\end{pmatrix}$ RMSE = 0.2697

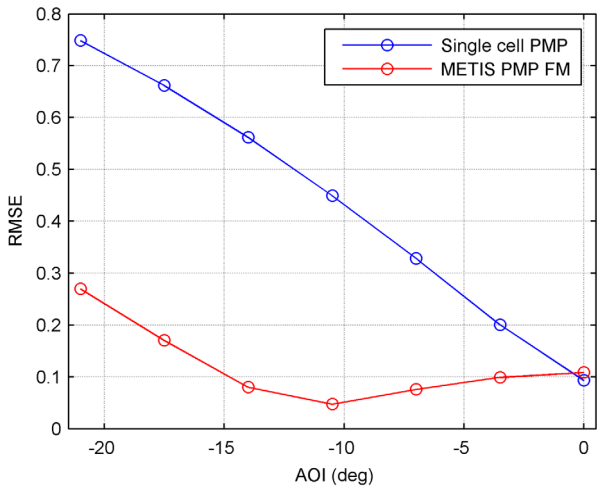

Fig. 10 RMSE of the modulation matrix O measured experimentally at a different AOI for PMP with single- and double-cell configurations.

polarizing elements (LCVRs, polarizers, QWP, etc.), imperfections of the LCVRs (optical activity, depolarization, etc.) are responsible for the nonideality found for the modulation matrix.

As the AOI is increased, both PMPs increase their RMSE, but the increase is drastically higher for the PMP with single-cell configuration. Note that, the PMP in the METIS coronagraph has to work with the AOI up to ± 7.0 deg. It is remarkable that until this value of angles, RMSE for the double-cell PMP keeps almost a constant value or is even reduced, whereas the RMSE for the single-cell PMP is more than three times its value at zero degrees.

The polarimetric efficiencies for both single- and double-cell configuration PMPs as a function of the AOI are shown in Fig. 11. As seen for the case of the modulation matrix, the dependence on the angle of incident is much higher for the single-cell PMP compared to the double-cell PMP.

As said previously, the ideal polarimetric efficiencies for the system are $[\varepsilon_1, \varepsilon_2, \varepsilon_4, \varepsilon_{\text{Total}}] = [1, 0.707, 0.707, 1]$. At zero degrees of the AOI, the efficiencies for single cell PMP are [0.9954, 0.6553, 0.6894, 0.9512], which corresponds to [99.5%, 92.7%, 97.5%, 95.1%] with respect to the ideal polarimetric efficiencies. For the double-cell PMP, the polarimetric efficiencies are [0.9998, 0.6662, 0.6889, 0.9583], which corresponds to [99.9%, 94.2%, 97.4%, 95.3%] with respect to the ideal polarimetric efficiencies. Therefore, both PMPs show very high polarimetric efficiencies, close to the ideal ones, at zero AOI.

Nevertheless, as the AOI is increased, noticeable changes are found for the case of the PMP with single-cell configuration. At -7 deg (the higher AOI for METIS PMP), the double-cell configuration does not show a significant change in its polarimetric efficiencies: [0.9996, 0.6603, 0.6868, 0.9527]. However, a significant change is obtained for the polarimetric efficiencies of the single-cell PMP: [0.9815, 0.5761, 0.7561,

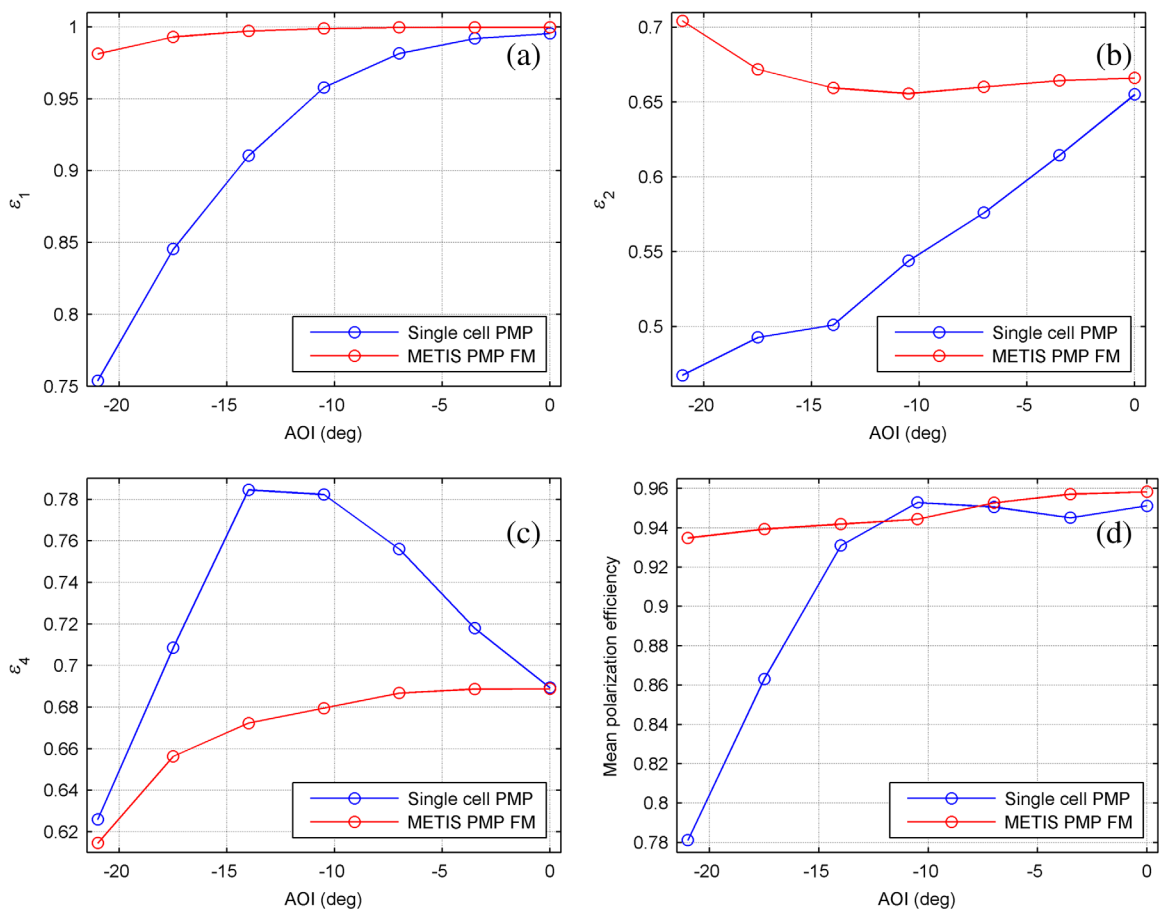

Fig. 11 Modulation efficiencies measured experimentally at a different AOI for PMP with single- and double-cell configuration. (a) ε_1, (b) ε_2, (c) ε_4, and (d) $\varepsilon_{\text{total}}$.

0.9506]. In this case, an unbalance of the efficiencies ε_2 and ε_4 occurs. ε_4 increases at the expense of ε_2, which involves an increase in the accuracy for the determination of circular polarization states (ε_4), with a consequent reduction in the accuracy for the determination of horizontal/vertical linear polarization states (ε_2). This effect is more remarkable as the AOI is increased.

Results in Secs. 4.1 and 4.2 show that the double-cell configuration used in METIS PMP show a much lower dependence on the AOI than the single-cell configuration, demonstrating the excellent performance of the functional concept of METIS PMP. Moreover, up to ± 7.0 deg of the AOI, which are the higher working incident angles of METIS coronagraph, the polarimetric performances of the double-cell PMP keep stable with slight variations, and a significant change is observed for the case of the single-cell configuration. Therefore, the METIS PMP concept using two LCVR cell with their molecular tilts in opposite directions guarantees an excellent maintenance of the polarimetric performances at the wide FOV expected in METIS coronagraph.

This fact in the context of METIS mission means that the same modulation matrix can be used for all the FOV, avoiding a nondesirable pixel per pixel calibration, which would increase the complexity of the data analysis and the resources needed on board the spacecraft. In addition, Stokes parameters of the incoming light will be determined with uniform polarimetric efficiencies and therefore uniform sensitivity along the entire FOV of METIS.

4.3 *Comparison Between Experimental and Model*

The comparison between experimental and theoretical modulation matrix for single- and double-cell PMPs as a function of the AOI is shown in Fig. 12. It can be observed that experimental and theoretical models agree successfully, especially for the case of double-cell configuration. For the case of single-cell configuration, some elements differ from the changes theoretically expected, but tendencies are the predicted. The same occurs with the polarimetric efficiencies shown in Fig. 13. For the case of the single-cell configuration, the changes are higher than expected, but tendencies agree successfully with the predicted model.

It is necessary to take into account that the theoretical model starts from a modulation matrix that gives maximum polarimetric efficiencies. This is not the case for the experimental data and could explain the differences observed with regard to the theoretical values. The nonidealities have not been considered in the model. Experimental deviations, such as thermal gradients along the LCVRs clear aperture, tilt, and azimuthal misalignments of the polarizing elements, imperfections of the LCVR cells (optical activity, depolarization, etc.) could are the responsible for the divergence from the theoretical data. These nonideality parameters must be analyzed thoroughly and separately in order to identify the contribution of each one in the modulation matrix and polarimetric efficiencies and its effect in the dependence on the AOI. This is beyond the scope of this paper and will be done in future works.

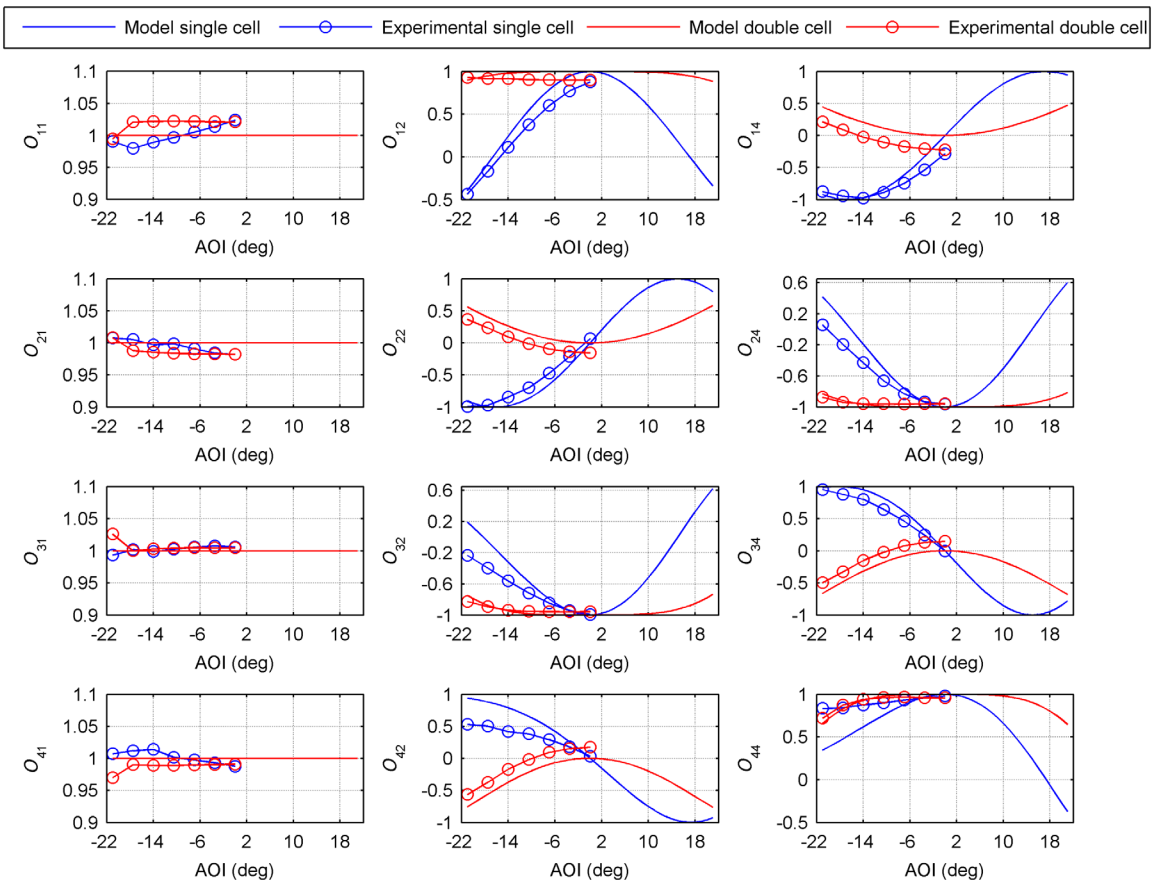

Fig. 12 Comparison between experimental and theoretical modulation matrix *O* elements of the PMPs with single- and double-cell configuration as a function of the AOI.

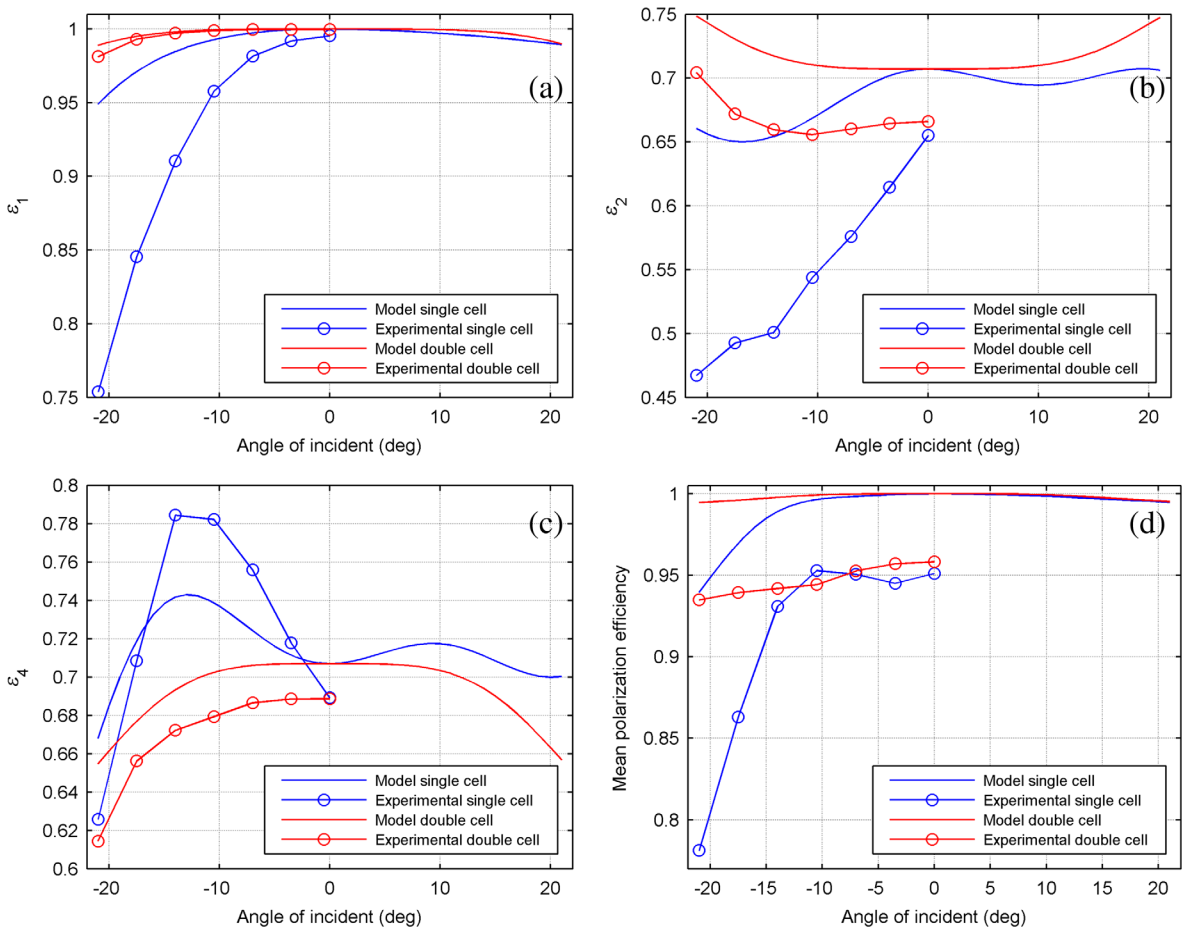

Fig. 13 Comparison between experimental and theoretical polarimetric efficiencies of the PMPs with single- and double-cell configuration as a function of the AOI. (a) ε_1, (b) ε_2, (c) ε_4, and (d) $\varepsilon_{\text{total}}$.

Nevertheless, the model shown in this paper allows predicting the behavior of each element of the modulation matrix, as well as the polarimetric efficiencies as a function of the AOI. This allows having very valuable information for the design of polarimetric instruments, such as coronagraphs, that present high FoVs.

4.4 *Wide Acceptance Angles for Other Polarimeters Configurations*

The demonstration that the model used fits experimental data allows us applying this model to polarimeters with other configurations. The model has been applied to a complete Stokes polarimeter with a dual configuration of two LCVR cells. In this configuration, the LCVR cells are placed with their optical axes properly oriented at 0 deg and 45 deg and with a modulation scheme (see Table 4) that gives maximum and uniform efficiencies, as specified in Eq. (5).

We have carried out different simulations. On the one hand, we compared the polarimetric performance of the LCVR cells in these azimuthal angles (0/45 deg) and placed them with their tilts in opposite and parallel directions. Different directions in the angular dependence can be calculated. In this case, the angular dependence was calculated for the extraordinary refractive index direction of the first LCVR cell (the cell at 0 azimuthal angle). This involves that the dependence on the second LCVR cell will be at 45 deg with regard to its extraordinary refractive

Table 4 Modulation scheme used for the complete Stokes polarimeter simulation.

Retardances (deg)	PM_1	PM_2	PM_3	PM_4
LCVR1 (azimuth = 0)	225	225	315	315
LCVR2 (azimuth = 45)	234.74	125.26	54.74	305.26

Table 5 Modulation scheme used for the complete Stokes polarimeter simulation (four LCVR cells configuration for wide acceptance angles).

Retardances (deg)	PM_1	PM_2	PM_3	PM_4
LCVR1 (azimuth = 0)	225/2	225/2	315/2	315/2
LCVR2 (azimuth = 0)	225/2	225/2	315/2	315/2
LCVR3 (azimuth = 45)	234.74/2	125.26/2	54.74/2	305.26/2
LCVR4 (azimuth = 45)	234.74/2	125.26/2	54.74/2	305.26/2

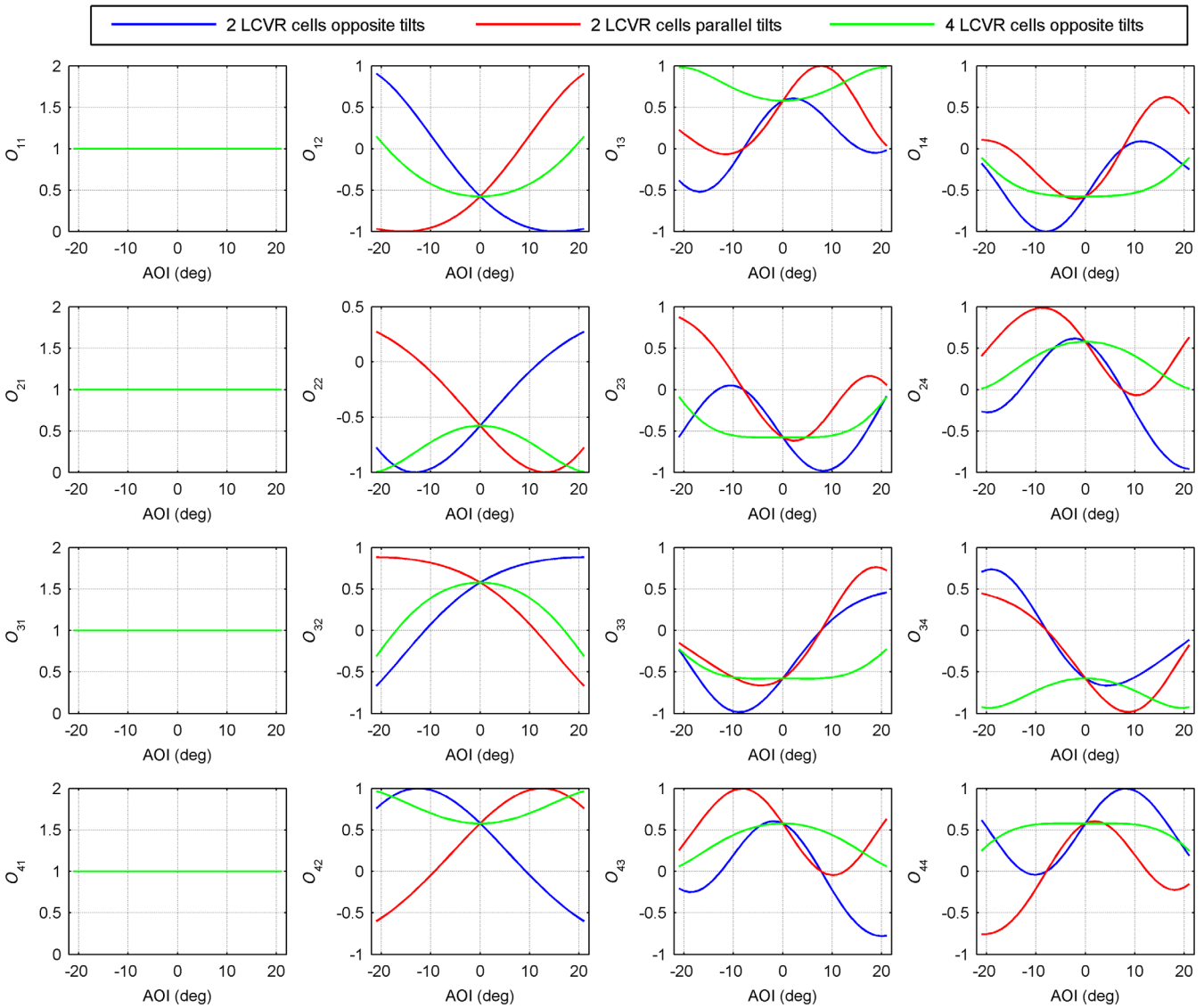

Fig. 14 Comparison of the modulation matrix O elements for the PMPs with azimuthal configuration of $0/45$ deg, in opposite and parallel tilts, and four LCVR cells configuration for wide acceptance angles (opposite tilts).

index. The simulations show that no reduction in the angular dependence is achieved by using opposite tilts compared to parallel tilts, because the reduction is achieved when the long axis (corresponding to the extraordinary refractive index) of the molecules of the two LCVR cells are aligned in the same direction and the molecules tilt in the opposite direction. For the configuration $0/45$ deg, the angular dependence reduction would be achieved by using four LCVR cells. Two LCVR cells at 0 deg with tilts in opposite directions and two LCVR cells at 45 deg with their tilts in opposite directions. As in METIS case, each cell would be modulated to half retardance to achieve the total retardance required for the modulation scheme (See Table 5). Figures 14 and 15 show the comparison of the polarimetric performance for the cases analyzed.

5 Conclusions

LCVRs will be used in the PMPs of the instruments SO/PHI and METIS of the Solar Orbiter Mission of the European Space Agency. The coronagraph of METIS will work with collimated beams and AOI up to ± 7.0 deg. For this reason, a configuration of double LCVR cell with molecular tilts in opposite directions was selected for METIS PMP, which provides lower angular dependence. The polarimetric performance of the flight model of METIS PMP has been measured at a different AOI up to -21 deg and compared to a single LCVR cell PMP. These measurements have been done along the extraordinary refractive index direction, which is the worst case.

The results shown in this paper demonstrate that the double-cell configuration used in METIS PMP show a much lower dependence on the AOI than the single-cell configuration. The polarimetric performances of the METIS PMP FM are almost kept constant up to ± 7.0 deg, which are the higher working incident angles of METIS coronagraph. Nevertheless, a noticeable change is found for the case of the single-cell configuration. This demonstrates the functional concept of METIS PMP and guarantees the maintenance of the

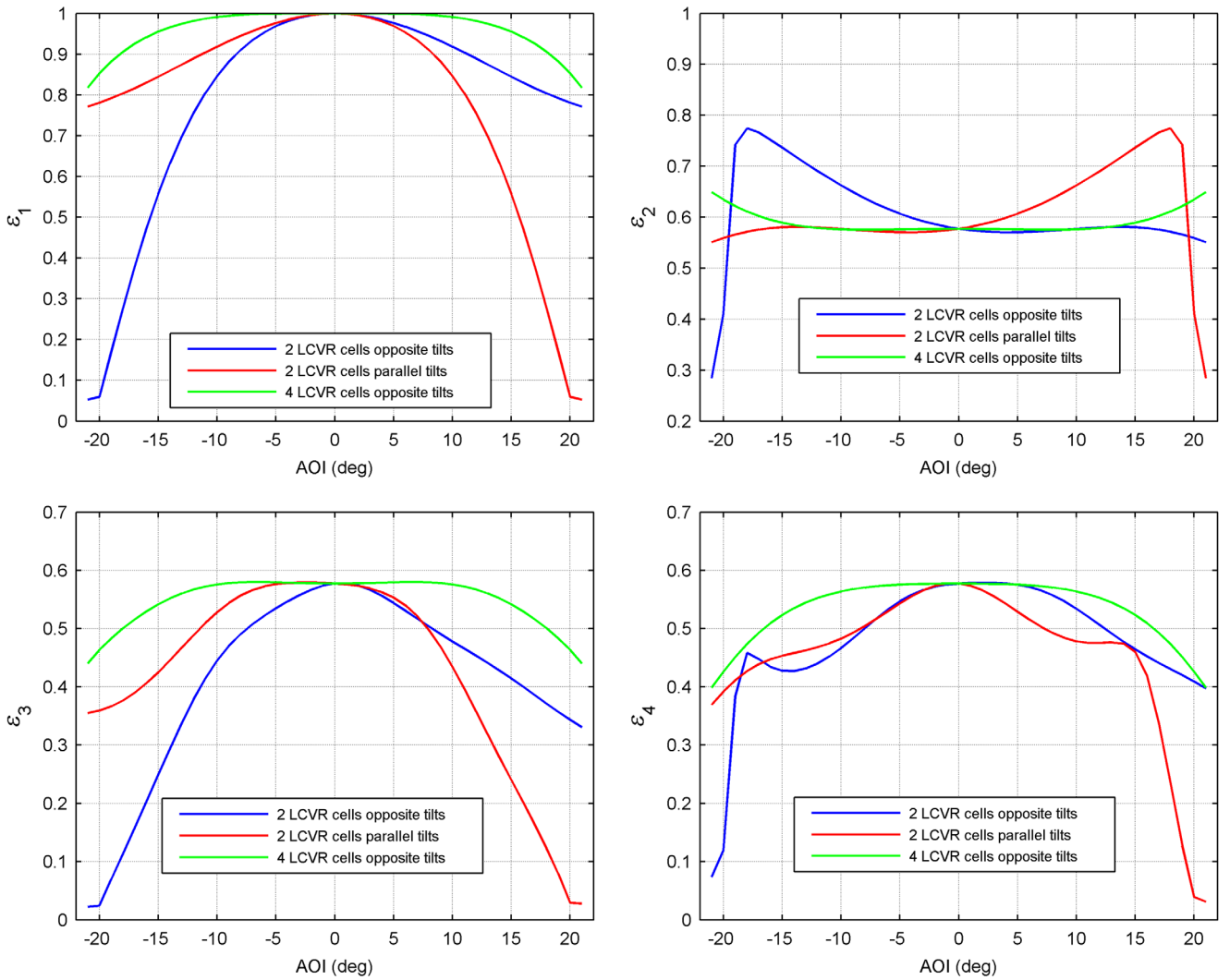

Fig. 15 Comparison of the polarimetric efficiencies of the PMPs with azimuthal configuration of 0/45 deg in opposite and parallel tilts and four LCVR cells configuration for wide acceptance angles (opposite tilts).

polarimetric performances at the wide FOV expected in METIS coronagraph.

Theoretical simulations have been also carried out. The modulation matrix and polarimetric efficiencies for both configurations (single- and double-cell PMPs) have been theoretically modeled as a function of the AOI along extraordinary and ordinary refractive index directions. They have been compared to the experimental data, finding successful agreement between theory and experimental measurements, especially for the case of double-cell PMP. Tendencies agree successfully although some changes are higher than predicted for single-cell PMP due probably to experimental deviations and imperfections of the LCVR cells (optical activity, depolarization, etc.) that have not been considered in this work. Nevertheless, the model shown in this paper allows predicting the behavior of the modulation matrix and polarimetric efficiencies as a function of the AOI. This is very helpful information that can be used for the design of other polarimetric instruments that present high FoVs, such as complete Stokes polarimeters, which has been also modeled in this work. Based on the work presented in this paper, researchers can select polarization modulators based on single- or double-LCVR cell configuration, depending on their instruments requirements.

Acknowledgments

The authors would like to express their gratitude to the INTA team for their technical support. Additionally, the authors gratefully acknowledge the financial support provided to this research by the MINECO (Ministerio de Economía y Competitividad, Gobierno de España), project ESP2016-77548-C5-4-R "Space Solar Physics: PHI for Solar Orbiter and IMaX and SP for Sunrise" and by the Agenzia Spaziale Italiana (ASI). Disclosures: The authors declare that they have no conflict of interest associated with this publication.

References

1. V. Martinez Pillet et al., "LPSP & TIP: full Stokes polarimeters for the Canary Islands observatories," in *High Resolution Solar Physics: Theory, Observations, and Techniques*, T. R. Rimmele, K. S. Balasubramaniam, and R. R. Radick, Eds., Astronomical Society of

the Pacific Conference Series, Vol. **183**, p. 264, Astronomical Society of the Pacific, San Francisco (1999).
2. A. Alvarez-Herrero et al., "Polarization modulators based on liquid crystal variable retarders for the solar orbiter mission," *Proc. SPIE* **9613**, 96130I (2015).
3. S. K. Solanki et al., "The polarimetric and helioseismic imager on solar orbiter," *A&A*, arXiv:1903.11061 (2019) (to be published).
4. E. Antonucci et al., "Metis: the solar orbiter visible light and ultraviolet coronal imager," *A&A* (2019) (to be published).
5. M. Silva-López et al., "Evaluation of a liquid crystal based polarization modulator for a space mission thermal environment," *Sens. Actuators A* **266**, 247–257 (2017)
6. Y. Itoh et al., "A double-layer electrically controlled birefringence liquid-crystal display with a wide-viewing-angle cone," *Jpn. J. Appl. Phys.* **30**, L1296–L1299 (1991).
7. H. Seki, Y. Masuda, and T. Uchida, "Optically compensated double-layer electrically controlled birefringence liquid crystal display with wide-viewing angle cone," *Liquid Crystals* **14**(2), 279–286 (1993).
8. N. Uribe-Patarroyo et al., "Space-qualified liquid-crystal variable retarders for wide-field-of-view coronagraphs," *Proc. SPIE* **8148**, 814810 (2011).
9. A. Hegyi and J. Martini, "Hyperspectral imaging with a liquid crystal polarization interferometer," *Opt. Express* **23**(22), 28742–28754 (2015).
10. J. C. del Toro Iniesta and M. Collados, "Optimum modulation and demodulation matrices for solar polarimetry," *Appl. Opt.* **39**(10), 1637–1642 (2000).
11. J. S. Tyo, "Design of optimal polarimeters: maximization of signal-to-noise ratio and minimization of systematic error," *Appl. Opt.* **41**(4), 619–630 (2002).
12. J. C. del Toro Iniesta and V. Martínez Pillet, "Assessing the behaviour of modern solar magnetographs and spectropolarimeters," *Astrophys. J. Suppl. Ser.* **201**, 22 (2012).
13. A. Alvarez-Herrero, P. García Parejo, and M. Silva-López, "Fine tuning method for optimization of liquid crystal based polarimeters," *Opt. Express* **26**(9), 12038–12048 (2018).
14. F. E. Veiras, L. I. Perez, and M. T. Garea, "Phase shift formulas in uniaxial media: an application to waveplates," *Appl. Opt.* **49**(15), 2769–2777 (2010).
15. P. García Parejo and A. Álvarez-Herrero, "Liquid crystals for space instrumentation: optical properties of liquid crystal mixtures for polarimeters," *Opt. Mat. Express* **9**(6), 2681–2698 (2019).

Pilar García Parejo graduated in chemistry at the Universidad Autonóma de Madrid (UAM), Spain, in 2003. She was awarded a PhD from UAM, researching on the preparation and characterization of sol–gel coatings for optical applications. Currently, she works in the space instrumentation area of INTA, Madrid. Her research interests are focused on the development and characterization of materials and optical devices to be used in payloads for space missions.

Alberto Álvarez-Herrero received his degree in fundamental physics and PhD from the Complutense University of Madrid (UCM), Spain, in 1994 and 2002, respectively. He has been at INTA since 1994, working in the development of space optical instrumentation. His research is aimed at new technologies, techniques, materials, and devices to be used in payloads for space missions. Ellipsometry and polarimetry are his main areas of expertise. Currently he is focused on liquid crystal devices, nanostructured coatings and effects of the space environment on the optical properties of materials.

Gerardo Capobianco is member of the Solar Physics Group at the Astrophysical Observatory of Torino of the Italian National Institute for Astrophysics. His research interests include the solar corona with development of innovative instrumentation for spectroscopic and polarimetric observations from Earth and in-flight. He is Co-I of the Metis instrument of the next ESA/Solar Orbiter Mission and Co-I of the ESA/PROBA-3 formation flying mission.

Silvano Fineschi is the director of the INAF-Astrophysical Observatory of Torino, Italy. He has 30 years of experience in space instrumentation for UV and visible-light spectroscopy and polarimetry. He has been involved in several solar space missions (e.g., SOHO, Solar Orbiter). Currently, he is the project scientist for the Metis coronagraph aboard Solar Orbiter and the principal investigator of the sounding-rocket coronagraphic experiment aboard a NASA suborbital mission. He is a lead scientist for the ASPIICS coronagraph aboard the ESA formation-flying mission PROBA-3.